Fangnon, Eric; Yagodzinskyy, Yuriy; Malictki, Evgenii; Mehtonen, Saara; Virolainen, Esa; Vilaça, Pedro

Determination of critical hydrogen concentration and its effect on mechanical performance of 2200 mpa and 600 hbw martensitic ultra-high-strength steel

Published in:
Metals

DOI:
10.3390/met11060984

Published: 20/06/2021

Document Version
Publisher's PDF, also known as Version of record

metals

MDPI

Article

Determination of Critical Hydrogen Concentration and Its Effect on Mechanical Performance of 2200 MPa and 600 HBW Martensitic Ultra-High-Strength Steel

Eric Fangnon [1,*], Yuriy Yagodzinskyy [1], Evgenii Malictki [1], Saara Mehtonen [2], Esa Virolainen [2] and Pedro Vilaça [1]

[1] Manufacturing and Materials, Department of Mechanical Engineering, School of Engineering, Aalto University, 02150 Espoo, Finland; yuriy.yagodzinskyy@aalto.fi (Y.Y.); evgeny.malitskiy@aalto.fi (E.M.); pedro.vilaca@aalto.fi (P.V.)

[2] SSAB, 92100 Raahe, Finland; saara.mehtonen@ssab.com (S.M.); esa.virolainen@ssab.com (E.V.)

* Correspondence: eric.a.fangnon@aalto.fi

Abstract: The influence of hydrogen on the mechanical performance of a hot-rolled martensitic steel was studied by means of constant extension rate test (CERT) and constant load test (CLT) followed with thermal desorption spectroscopy measurements. The steel shows a reduction in tensile strength up to 25% of ultimate tensile strength (UTS) at critical hydrogen concentrations determined to be about 1.1 wt.ppm and 50% of UTS at hydrogen concentrations of 2 wt.ppm. No further strength degradation was observed up to hydrogen concentrations of 4.8 wt.ppm. It was observed that the interplay between local hydrogen concentrations and local stress states, accompanied with the presence of total average hydrogen reducing the general plasticity of the specimen are responsible for the observed strength degradation of the steel at the critical concentrations of hydrogen. Under CLT, the steel does not show sensitivity to hydrogen at applied loads below 50% of UTS under continuous electrochemical hydrogen charging up to 85 h. Hydrogen enhanced creep rates during constant load increased linearly with increasing hydrogen concentration in the steel.

Keywords: hydrogen embrittlement; ultra-high-strength steels; thermal desorption spectroscopy; constant extension rate test; constant load test

check for updates

Citation: Fangnon, E.; Yagodzinskyy, Y.; Malictki, E.; Mehtonen, S.; Virolainen, E.; Vilaça, P. Determination of Critical Hydrogen Concentration and Its Effect on Mechanical Performance of 2200 MPa and 600 HBW Martensitic Ultra-High-Strength Steel. *Metals* **2021**, *11*, 984. https://doi.org/10.3390/met11060984

Academic Editor: João Pedro Oliveira

Received: 26 May 2021
Accepted: 16 June 2021
Published: 20 June 2021

1. Introduction

There is an ever-increasing need for hard and tough steels for demanding wear and impact resistance industrial applications. These include mining equipment in severe corrosion environments [1], ballistic resistance in armored and patrol vehicles, and protected buildings in civil construction [2]. As the need for safe operation of higher strength steels for challenging applications is increasing, so are concerns about their susceptibility to hydrogen. Over the years, several industrial failures related to hydrogen have been reported ranging from small components such as fasteners to large ones like boilers, hydrogen storage tanks, oil, and gas structures [3,4]. Hydrogen interacts with metallic materials in a way that reduces their ductility, toughness and even their strength [5]. It has been reported that local stresses and local hydrogen concentrations are controlling factors of the loss of fracture strength in steels [6]. The primary conditions responsible for the undesired failure depend often on dislocation process, and are controlled by hydrogen diffusion and trapping, coupled with the state of stresses in the material [7–9].

Generally, the susceptibility of steels to hydrogen increases with their strength [10–13]. As steels are produced with increased strength, they become harder, less ductile, less tough, and more susceptible to hydrogen embrittlement (HE). The susceptibility of quenched and tempered ferritic-martensitic steels increases significantly above 1200 MPa with hardness of about 360 HBW [14]. To a large extent, this can be attributed to two phenomena. One

is the high diffusivity of hydrogen in ferritic-martensitic steels [15]. The other is the segregation of alloying elements resulting from the high alloying and high carbon content used for hardening, leading to the formation of carbides and precipitates that act as stress concentrators, affecting the diffusion and trapping of hydrogen in these materials. Over the years, HE mechanisms such as hydrogen enhanced decohesion (HEDE), and hydrogen enhanced localized plasticity (HELP) have been proposed as damage mechanisms in steels in the presence of hydrogen. The HEDE mechanism suggests that embrittlement is due to localized reduction in cohesive strength of the iron lattice in hence assists the separation of cleavage planes or grain boundaries under lower stresses [16,17]. While the HELP mechanism focuses on the fact that atomic hydrogen accelerate the dislocation mobility through an elastic shielding effect that causes a local reduction in shear stress and hydrogen transport by dislocation motion, which could lead to localized high concentrations at distances further ahead of crack tip [7,18,19].

The evaluation of the hydrogen embrittlement property of steels, particularly new ultra-high strength steels, is an important task allowing their safe and reliable use in conditions under which their susceptibility to hydrogen is found to be minimal. This is a difficult task to perform because many variables considering that factors like chemistry, microstructure, metallurgical defects, operating temperatures, and stress states simultaneously affect the sensitivity of steel to hydrogen. It is widely reported in literature [20–24] that the degradation of mechanical properties of steels in the presence of hydrogen occurs only when hydrogen reaches a certain critical concentration in the steel. Hence the critical hydrogen concentration (H_{crit}) was proposed as a parameter to evaluate the hydrogen embrittlement property of high-strength steels [23,24].

It has been determined that tensile strength of steels decreases with increasing diffusible hydrogen content leading to the formulation of a power law relationship between fracture strength and diffusible hydrogen content [25]. However, it was also observed the power law was not always applicable, especially for notched specimens. The strong dependence of the notch tensile strength on the stress intensity factor makes it unlikely to be used as fracture criterion for HE, except for specified geometries [6,25]. In addition, it was found that the power law relationship between fracture stress and hydrogen content is mostly applicable only when the fracture mode is intergranular [26] limiting its application to various steels with complex microstructures. In recent years, many studies have explored promising H-resistant additively manufactured steels [27,28]. However, until their full development, conventionally manufactured ultra-high-strength, hard and impact resistant steels are still the primary options.

Slow strain rate tests has been used in several studies to evaluate the effect of hydrogen on mechanical properties of steels, the technique is believed to allow enough time for hydrogen activity within the material [22]. Although SSRT and hydrogen concentration measurement techniques have been employed in several studies to determine H_{crit} for high-strength steels up to 1500 MPa [29–34], much more work is still required. Particularly in determining H_{crit} for higher strength steels (>1500 MPa) and its effect on the mechanical performance of these steels under constant loads, focusing specifically on the hydrogen enhanced creep rates.

In this study, we determine the critical hydrogen concentration and evaluate its effect on the mechanical performance of a modern steel for demanding applications. The material is a martensitic ultra-high-strength steel (2200 MPa), with hardness of 600 HBW. The research methods include constant extension rate testing (CERT), constant load testing (CLT), hydrogen thermal desorption spectroscopy (TDS), and fractography.

2. Materials and Methods

2.1. Material

A hot-rolled and quenched medium carbon steel with ultimate tensile strength of 2200 MPa and hardness of 600 HBW (58 HRC) was studied. The steel was obtained from steel manufacturer SSAB, in Finland. An optical microscopic observation of the studied

Metals **2021**, *11*, x FOR PEER REVIEW 3 of 16

steel (after etching with Nital 2% for 20 s) shows a dominant martensitic microstructure with islands of bainite as shown in Figure 1. The relevant major chemical composition and the mechanical properties of the studied steel are summarized in Table 1.

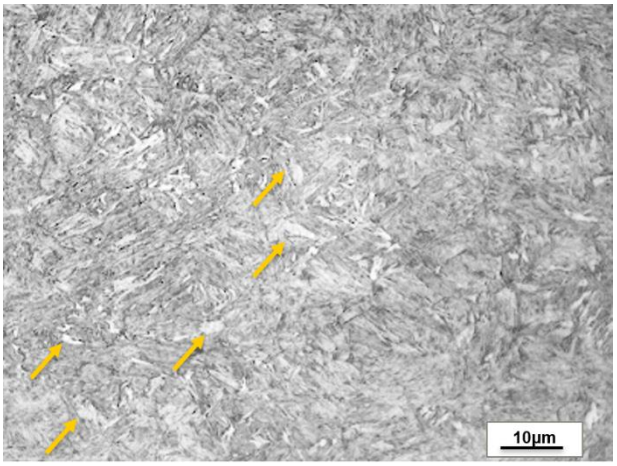

Figure 1. Microstructure of the studied steel showing dominantly a martensitic microstructure with bainitic islands indicated by yellow arrows (after etching with Nital 2% for 20 s).

Table 1. Chemical composition and mechanical properties of the studied steel.

Steel Composition [wt.%]			Mechanical Properties		
C	0.370	0.370	UTS [MPa]	2200	2200
Mn	0.299	0.299	YS, at 2% offset [MPa]	1800	1800
S	0.001	0.001	Measured hardness [HBW]	600	600
Al	0.430	0.430	Elongation at fracture [%]	12	12

2.2. Specimen Preparation

Two types of specimens were used in the study. TDS specimens with characteristic size of 1 mm × 4 mm × 10 mm were used for investigation of hydrogen charging parameters and hydrogen uptake of the steel. Secondly, sub-sized specimens were used for mechanical tensile testing (MT) with size of 5 mm × 10 mm × 300 mm and gauge part size of 1.0 mm × 5.0 mm × 20 mm, shown in Figure 2a. All the specimens were cut by EDM and polished mechanically finishing with emery paper No. 1200. Additionally, the MT specimens were Teflon-taped to expose only the gauge part to hydrogen charging, as shown in Figure 2b.

2.3. Hydrogen Charging

Electrochemical hydrogen charging was performed in a glass, three-electrode electrochemical cell combined with a Gamry potentiostat framework. Calomel reference electrode and platinum wire counter electrode were used in the cell together with the steel specimen as the working electrode.

To obtain a suitable hydrogen charging parameters for the studied steel, the TDS specimens were charged from 3% of NaCl and 0.1% NH_4SCN as hydrogen atom recombination poison [35]. The charging time was varied from 10 min to 12 h at an applied electrochemical potential of −1 V_{SCE}, followed with hydrogen concentration measurement using TDS method. Hydrogen uptake of the studied steel as a function of the applied electrochemical potentials was also measured by varied potential from −0.8 to −1.3 V_{SCE} for a charging time of 2 h.

Metals **2021**, *11*, x FOR PEER REVIEW 4 of 16

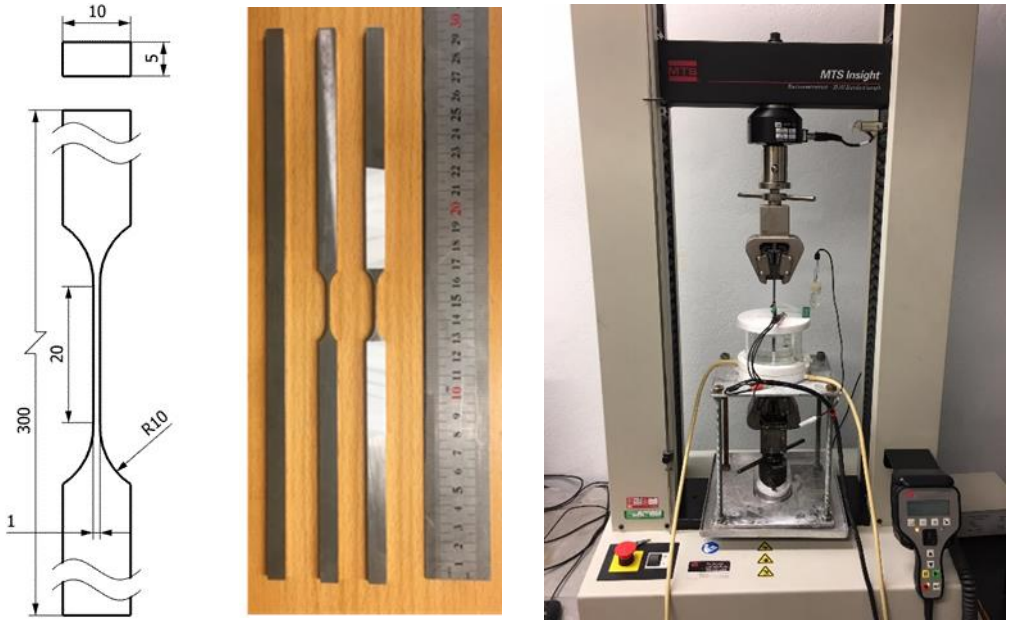

(**a**) (**b**) (**c**)

Figure 2. (**a**) Dimensions of mechanical testing (MT) specimens; (**b**) MT specimens prior to H-charging; (**c**) assembly of MT specimen with the electrochemical cell and loading unit for tensile testing (CERTs and CLTs) under continuous H-charging.

2.3. Hydrogen Charging

The MT specimens were H-charged electrochemically from 3% NaCl + 0.1% and 0.3% NH_4SCN for 2 h determined from the charging time dependency of the hydrogen concentration when the concentration plot approaches saturation, which corresponds to almost homogeneous distribution of hydrogen across the thickness of the specimen's gauge part. The applied electrochemical potential for hydrogen charging was varied between −0.8 to −1.4 V_{SCE}. A combination of the applied potential and H-charging poison content was used to provide a rather wide range of hydrogen concentration in the MT specimens.

The pH of the electrolyte was measured to be 5.5 and 4.5 for the electrolyte solution containing 0.1% and 0.3% NH_4SCN, respectively. The electrolyte is replaced with a fresh one if the pH changes due to evaporation of the solution over the testing time. During H-charging, the electrolyte was kept under constant stirring and deaeration by nitrogen gas flow. Hydrogen charging was performed at room temperature, about 20 °C.

2.4. Mechanical Testing

After 2 h of hydrogen pre-charging, mechanical testing comprising of CERT and CLT is initiated under continuous hydrogen charging. CERTs were performed with a 30 kN MTS benchtop tensile test machine at the strain rate 10^{-4} s^{-1} and CLTs at the same strain rate until the applied load was attained. In the case of CLT, mechanical testing was stopped, if fracture does not occur after 85 h under applied load and continuous hydrogen charging. Figure 2c shows a general view of mechanical testing setup with continues hydrogen charging.

After fracture or abortion of testing, the gauge part of the MT specimen was cut into two parts. One is cut to the characteristic size of a TDS specimen and taken for hydrogen concentration measurement with TDS. The other is cleaned with distilled water and stored for fractography in a vacuum chamber to prevent the formation of any oxide layers.

stopped, if fracture does not occur after 85 h under applied load and continuous hydrogen charging. Figure 2c shows a general view of mechanical testing setup with continues hydrogen charging.

After fracture or abortion of testing, the gauge part of the MT specimen was cut into two parts. One is cut to the characteristic size of a TDS specimen and taken for hydrogen concentration measurement with TDS. The other is cleaned with distilled water and stored for fractography in a vacuum chamber to prevent the formation of any oxide layers.

2.5. Hydrogen Concentration Measurement

The TDS apparatus used for hydrogen measurement was designed, manufactured, and assembled at Aalto University, Finland. The general schematic view of the TDS apparatus is shown in Figure 3.

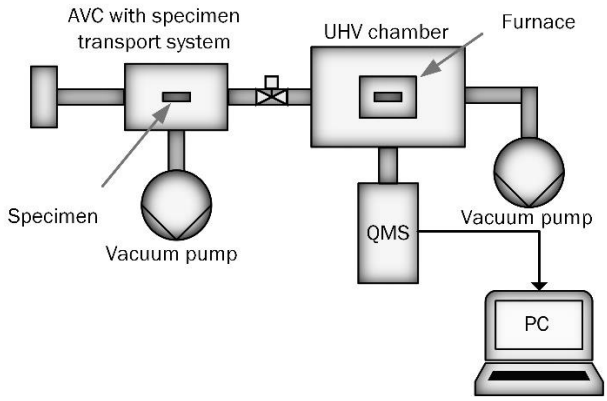

Figure 3. Schematic view of the thermal desorption spectroscopy apparatus.

Before TDS measurement the specimens were cleaned with distilled water followed by drying in helium gas flow to prevent any effect of moisture on the TDS measurement. The measurement of partial pressure of hydrogen occurs in the UHV chamber (1×10^{-9} mbar) coupled with a mass spectrometer (SRS residual gas analyser RGA100). To keep the UHV chamber at the required pressure and reduce pumping time before measurement, the sample was first placed in an airlock compartment and pumped to an intermediate pressure of 1×10^{-6} mbar. After which the specimen was transported to the UHV chamber and measurement initiated. The total time from the specimen preparation, placing it in the airlock, transporting it to the furnace in the UHV chamber did not exceed 10 min [15]. All TDS measurements performed at a heating rate of 10 K/min.

3. Results

3.1. Hydrogen Uptake

To determine hydrogen charging conditions suitable for tensile testing, the hydrogen uptake of the steel was evaluated by a combination of three methods. Firstly, the hydrogen uptake was measured as a function of electrochemical charging time as depicted in Figure 4a. The measured hydrogen concentration increased with increasing charging time up to 1.45 wt.ppm at 3.5 h. Upon fitting the experimental results with an exponential growth curve, it is possible to conclude that after 2 h, it approaches a certain plateau of average hydrogen concentration. Thus, a charging time of 2 h was selected to be the characteristic charging time. This charging time is considered enough to provide an almost homogeneous distribution of hydrogen in the steel specimen.

In addition, the dependency of hydrogen uptake on the applied electrochemical potential was evaluated. Figure 4b shows the measured average hydrogen concentration as a function of applied potential after 2 h of H-charging. At the employed testing conditions, hydrogen concentration increases with the increase of applied potential up to -1.3 V_{SCE}, after which a further increase of applied potential resulted in a decrease of measured hydrogen concentration. Lastly, the effect of the concentration of NH_4SCN in the electrolyte was determined. At a controlled applied potential of -1.2 V_{SCE} the increase of NH_4SCN in the electrolyte from 0.1% to 0.3% results in an increase of measured hydrogen concentration 2.25 to 3.3 wt.ppm, as shown in Figure 4c. An appropriate combination of applied potential and NH_4SCN concentration allows for a controlled amount of hydrogen concentration in the tested specimen [35].

after which a further increase of applied potential resulted in a decrease of measured hydrogen concentration. Lastly, the effect of the concentration of NH_4SCN in the electrolyte was determined. At a controlled applied potential of −1.2 V_{SCE} the increase of NH_4SCN in the electrolyte from 0.1% to 0.3% results in an increase of measured hydrogen concentration 2.25 to 3.3 wt.ppm, as shown in Figure 4c. An appropriate combination of applied potential and NH_4SCN concentration allows for a controlled amount of hydrogen concentration in the tested specimen [35].

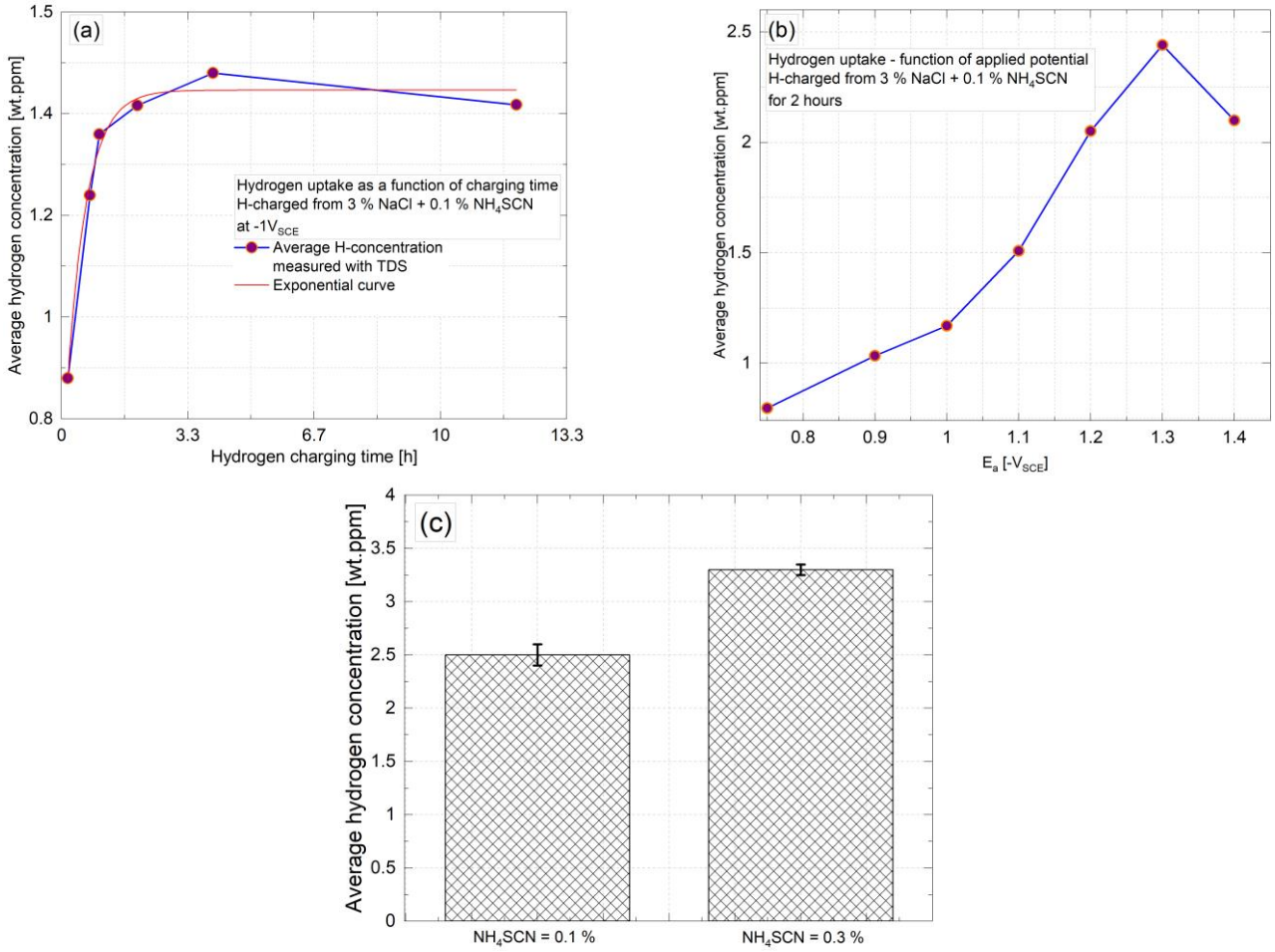

Figure 4. (a) Measured hydrogen concentration as a function of hydrogen charging time; (b) measured hydrogen concentration as a function of applied electrochemical potential; (c) effect of NH_4SCN concentration on the measured hydrogen concentration after hydrogen charging for 2 h at the applied potential of −1.2 V_{SCE}.

3.2. Constant Extention Rate Test (CERT)

Constant extension rate tests were performed under continuous hydrogen charging of the studied steel after 2 h of pre-charging. After MT specimen fracture, the hydrogen content is measured by TDS as described in Section 2. Hydrogen effect on tensile properties of the studied steel is shown Figure 5a. The steel manifests a sensitivity to hydrogen not only within plastic deformation range at lower hydrogen concentrations, but also within the elastic range which results in fracture at stresses below the yield point for higher hydrogen concentrations. The engineering stress–strain curves manifest a remarkable loss of strength and elongation to fracture with the increase of hydrogen concentrations. Hydrogen concentrations of about 0.65, 1.1, and 3.75 wt.ppm in the steel sample result in fracture stresses of 2100, 1630, and 1100 MPa, respectively.

Constant extension rate tests were performed under continuous hydrogen charging of the studied steel after 2 h of pre-charging. After MT specimen fracture, the hydrogen content is measured by TDS as described in Section 2. Hydrogen effect on tensile properties of the studied steel is shown Figure 5a. The steel manifests a sensitivity to hydrogen not only within plastic deformation range at lower hydrogen concentrations, but also within the elastic range which results in fracture at stresses below the yield point for higher hydrogen concentrations. The engineering stress–strain curves manifest a remarkable loss of strength and elongation to fracture with the increase of hydrogen concentrations. Hydrogen concentrations of about 0.65, 1.1, and 3.75 wt.ppm in the steel sample result in fracture stresses of 2100, 1630, and 1100 MPa, respectively.

The reduction of the fracture stress during CERT of the studied steel as a function of the hydrogen concentration is shown in Figure 5b. The strength of the steel reduces from an apparent upper plateau for small hydrogen contents to a clear lower plateau at about 1100 MPa for higher hydrogen concentrations up to 4.8 wt.ppm. The observed lower plateau can be considered as the maximum hydrogen effect on the UTS of the studied steel. The hydrogen concentration of about 1.1 wt.ppm corresponding to the midpoint between the upper and lower plateau can be considered the critical hydrogen concentration

(Hc_{crit}) [21]. An analytical representation of the critical hydrogen concentration can be described with an 'atan' function in form of Equation (1):

$$Y = Y_0 + A \times atan[(X - X_c)/W], \tag{1}$$

where X is the measured hydrogen concentration and $Y_0 = 1657$, $A = -412$, $X_c = 1.05$, $and\ W = 0.2$ are the best fitting parameters generated automatically by the OriginPro software. The fitted curve corresponds well with the experimentally obtained results with an accuracy of $R^2 = 0.96$ as shown in Figure 5b. Notably, $X_c = 1.05$ corresponds to the critical hydrogen concentration. The hydrogen embrittlement index (EI) which is about 50% for the studied steel was calculated by Equation (2) [36]:

$$EI = \frac{UTS_{air} - UTS_{H(plateau)}}{UTS_{air}} \times 100\%, \tag{2}$$

where $UTS_{air} = 2200$ MPa is the ultimate tensile strength of the steel tested in air, and $UTS_{H(plateau)} = 1100$ MPa is the ultimate tensile strength of the steel tested under continuous hydrogen charging corresponding to the lower plateau on the hydrogen embrittlement curve.

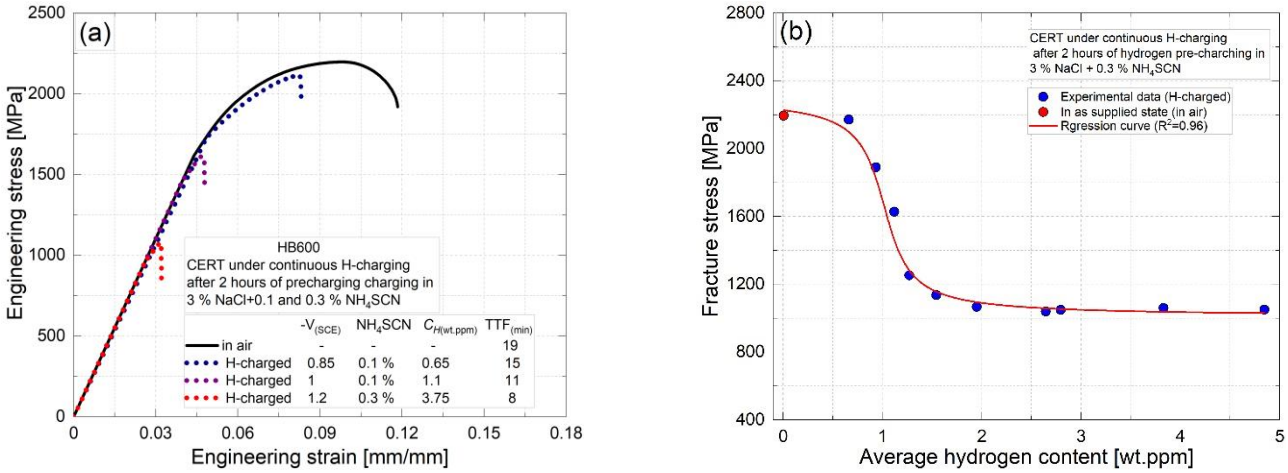

Figure 5. (**a**) Engineering stress versus strain curves of studied steel showing the effect of hydrogen on the tensile property of studied steel; (**b**) hydrogen embrittlement curve of tested steel showing a clear lower plateau at 1100 MPa.

TDS hydrogen measurements were performed after the CERT. The thermal desorption curves for specimens fractured at 1630 and 1100 MPa, with corresponding hydrogen concentrations of 1.1 wt.ppm (curve 1) and 3.75 wt.ppm (curve 2), are shown in Figure 6. The complex curves have clearly two components: A distinctive lower temperature component (325 to 550 K) and a higher temperature component (550 to 1000 K). Curve 1 shows two visible peaks, a characteristic lower temperature peak at 460 K followed by a broader higher temperature peak at 631 K. Curve 2 shows visible peaks consisting of a lower temperature peak at 450 K, complex broad higher temperature peaks at 670 K and 890 K. The characteristic of curves 1 and 2 are common for high-strength steels after deformation under CERT [37]. For both curves 1 and 2, the lower temperature components of the TDS spectra are preferably associated with the hydrogen trapping in microstructural defects in the solid solution such as dislocations, grain boundaries, vacancies, and nano-voids [38]. While the higher temperature components are associated with the decomposition of the molecular hydrogen trapped in voids during the metallurgical processes [39].

The reduction of the fracture stress during CERT of the studied steel as a function of the hydrogen concentration is shown in Figure 5b. The strength of the steel drops from an apparent upper plateau for small hydrogen contents to a clear lower plateau at about 1100 MPa for higher hydrogen concentrations up to 4.8 wt.ppm. The observed lower plateau can be considered as the maximum hydrogen effect on the UTS of the studied steel. The hydrogen concentration of about 1.1 wt.ppm corresponding to the midpoint between the upper and lower plateau can be considered the critical hydrogen concentration (Hc_{crit}) [21]. An analytical representation of the critical hydrogen concentration can be described with an 'atan' function in form of Equation (1):

$$Y = Y_0 + A \times atan[(X - X_c)/W], \tag{1}$$

where X is the measured hydrogen concentration and $Y_0 = 1657, A = -412, X_c = 1.05, and\ W = 0.2$ are the best fitting parameters generated automatically by the OriginPro software. The fitted curve corresponds well with the experimentally obtained results with an accuracy of $R^2 = 0.96$ as shown in Figure 5b. Notably, $X_c = 1.05$ corresponds to the critical hydrogen concentration. The hydrogen embrittlement index (EI) which is about 50% for the studied steel was calculated by Equation (2) [36]:

$$EI = \frac{UTS_{air} - UTS_{H(plateau)}}{UTS_{air}} \times 100\%, \tag{2}$$

where $UTS_{air} = 2200$ MPa is the ultimate tensile strength of the steel tested in air, and $UTS_{H(plateau)} = 1100$ MPa is the ultimate tensile strength of the steel tested under contin-

crostructural defects in the solid solution such as dislocatio
cies, and nano-voids [38]. While the higher temperature con
the decomposition of the molecular hydrogen trapped in vo
processes [39].

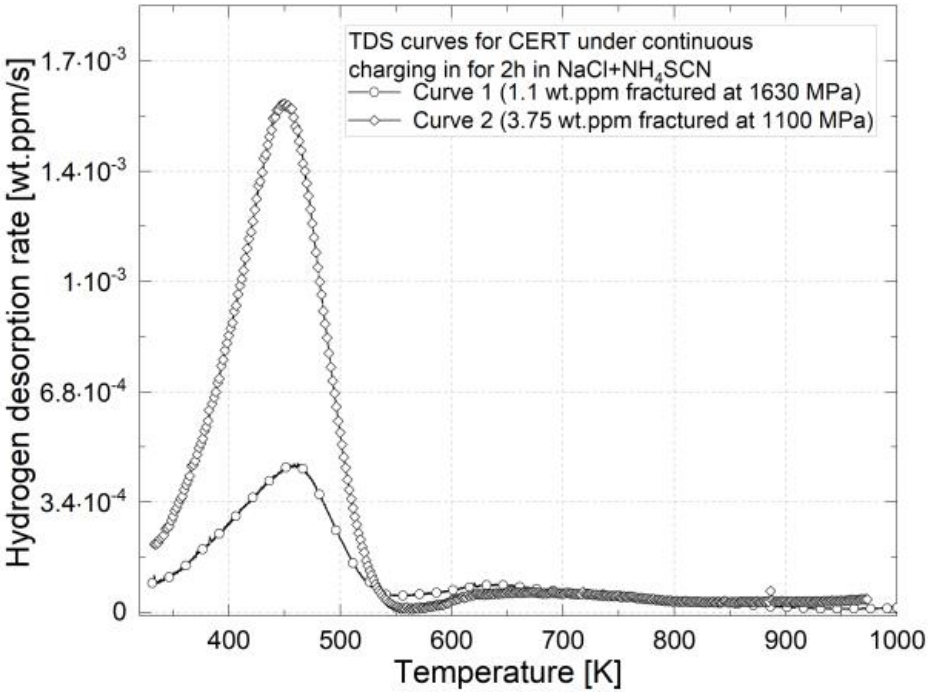

Figure 6. TDS curves for specimens after CERT under continuou
fractured at 1650 MPa with corresponding hydrogen concentratio
1100 MPa with 3.75 wt.ppm (**curve 2**). Heating rate 10 K/min.

3.3. Constant Load Tests (CLTs)

CLTs were performed at varying applied constant loads with MT specimens in air and under continuous electrochemical hydrogen charging at conditions that correspond to the critical hydrogen concentration determined during CERT (i.e., 3% NaCl + 0.1% NH_4SCN at about −1 V_{SCE}). The actual time to fracture in CLTs was calculated as overall testing time excluding the time taken to attain the actual applied load. Loads at which fracture does not occur after 85 h under load are considered having reached a 'safe zone' and the test is aborted. The applied load as a function of time to fracture for specimens under continuous hydrogen charging is shown in Figure 7. The susceptibility of the steel to hydrogen under constant load is evident as the applied load and time to fracture shows a linear correlation on a semi-logarithmic scale. For example, the hydrogen-free specimen reaches the 'safe zone' (no fracture after 85 h) at applied stress of 1600 MPa (72% of UTS) while the samples under continuous hydrogen charging fractures in about 2 min under the same load. The H-charged specimen reaches the 'safety zone' at an applied stress of 1100 MPa (50% of UTS).

In addition, the effect of hydrogen on the hydrogen-enhanced creep in CLT was evaluated. A typical creep curve obtained from the CLT data of the studied steel (applied load 1400 MPa) is shown in Figure 8a where the derivative of the stage II of the creep curve is considered as the creep rate [40]. The creep rates linearly increase with increasing total hydrogen concentration, as shown in Figure 8b.

3.4. Fractography

Fractographic observations were made after CERT in air, hydrogen charged to the critical concentration, and hydrogen charged above the critical concentrations. As shown in Figure 9a, the fracture surface manifests a ductile fracture characterized by dimpled rupture for the specimen tested in air. At increasing hydrogen concentrations around the critical range, the fracture surface shows a brittle fracture area with clearly visible long secondary cracks, as emphasized in Figure 9b. At hydrogen concentrations corresponding

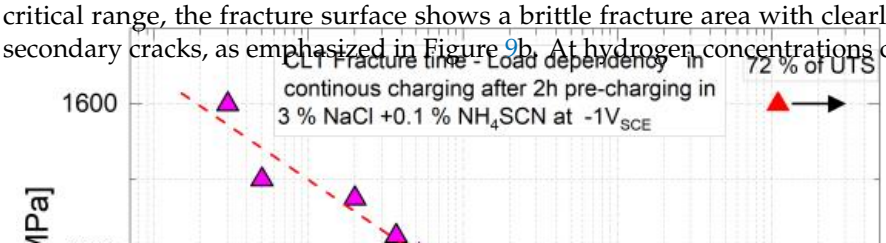

CLTs were performed at varying applied constant loads
under continuous electrochemical hydrogen charging at cond
critical hydrogen concentration determined during CERT (i.e
about −1 V_{SCE}). The actual time to fracture in CLTs was calc
excluding the time taken to attain the actual applied load. Loa
occur after 85 h under load are considered having reached
aborted. The applied load as a function of time to fracture for
hydrogen charging is shown in Figure 7. The susceptibility o
constant load is evident as the applied load and time to fract
on a semi-logarithmic scale. For example, the hydrogen-fre
zone' (no fracture after 85 h) at applied stress of 1600 MPa (72
under continuous hydrogen charging fractures in about 2 min
charged specimen reaches the 'safety zone' at an applied stres

occur after 85 h under load are considered having reached
aborted. The applied load as a function of time to fracture fo
hydrogen charging is shown in Figure 7. The susceptibility o
constant load is evident as the applied load and time to fract
on a semi-logarithmic scale. For example, the hydrogen-fr
zone (no fracture after 85 h) at applied stress of 1600 MPa (7
under continuous hydrogen charging fractures in about 2 mi
charged specimen reaches the 'safety zone' at an applied stre

to the plateau above the critical concentration, the fracture surface shows a fine blend of transgranular and intergranular fracture mode, with high-density of secondary cracks forming most likely along the prior austenite grain boundaries, as emphasized in Figure 9c.

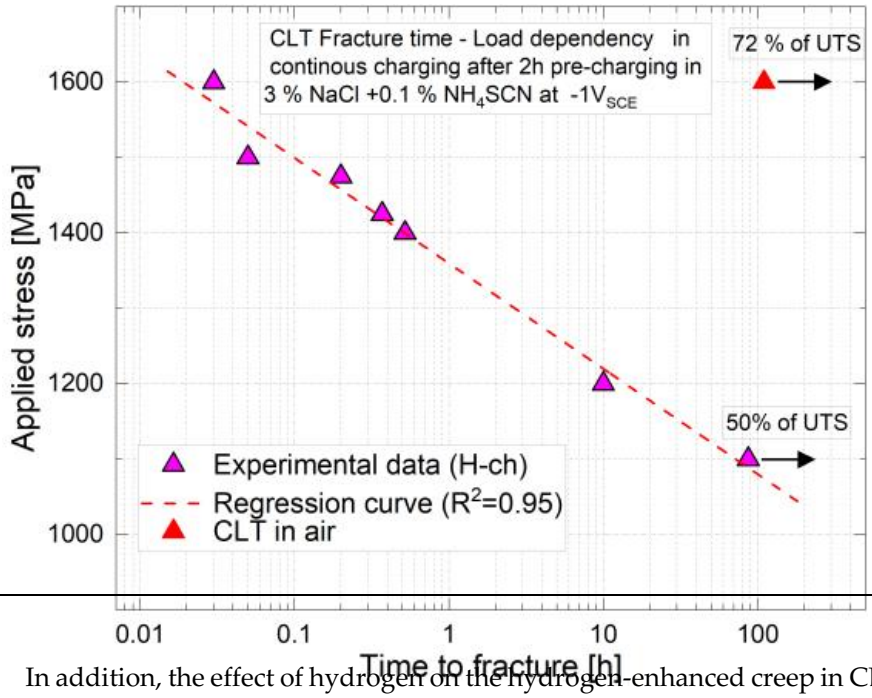

Figure 7. CLT-based results with applied load as a function of time to fracture. The CLT of hydrogen charged specimens are performed at continuous hydrogen charging, after 2 h of pre-charging under conditions corresponding to the critical hydrogen concentrations.

In addition, the effect of hydrogen on the hydrogen-enhanced creep in CLT was evaluated. A typical creep curve retrieved from the CLT data of the studied steel (applied load 1400 MPa) is shown in Figure 8a where the derivative of the stage II of the creep curve is considered as the creep rate [40]. The creep rate linearly increases with increasing total hydrogen concentration, as shown in Figure 8b.

charged specimens are performed at continuous hydrogen chargin
conditions corresponding to the critical hydrogen concentrations.

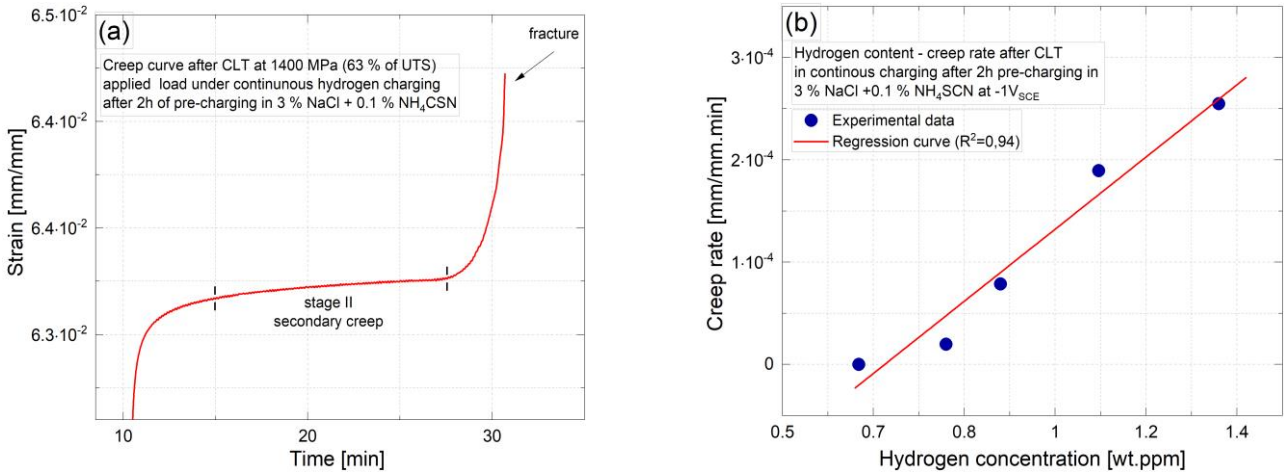

Figure 8. (**a**) Engineering strain versus time curve from CLT at 1400 MPa under continuous hydrogen charging; (**b**) creep rates as a function of hydrogen concentration.

3.4. Fractography

Fractographic observations were made after CERT in air, hydrogen charged to the critical concentration, and hydrogen charged above the critical concentrations. As shown in Figure 9a, the fracture surface manifests a ductile fracture characterized by dimpled rupture for the specimen tested in air. At increasing hydrogen concentrations around the critical range, the fracture surface shows a brittle fracture area with clearly visible long secondary cracks, as emphasized in Figure 9b. At hydrogen concentrations corresponding to the plateau above the critical concentration the fracture surface shows a fine blend of transgranular and intergranular fracture mode, with high-density of secondary cracks

rupture for the specimen tested in air. At increasing hydrogen concentrations around the critical range, the fracture surface shows a brittle fracture area with clearly visible long secondary cracks, as emphasized in Figure 9b. At hydrogen concentrations corresponding to the plateau above the critical concentration the fracture surface shows a fine blend of transgranular and intergranular fracture mode, with high-density of secondary cracks forming most likely along the former austenite grain boundaries as well as martensitic lath, as depicted in Figure 9c.

Metals **2021**, *11*, x FOR PEER REVIEW 10 of 16

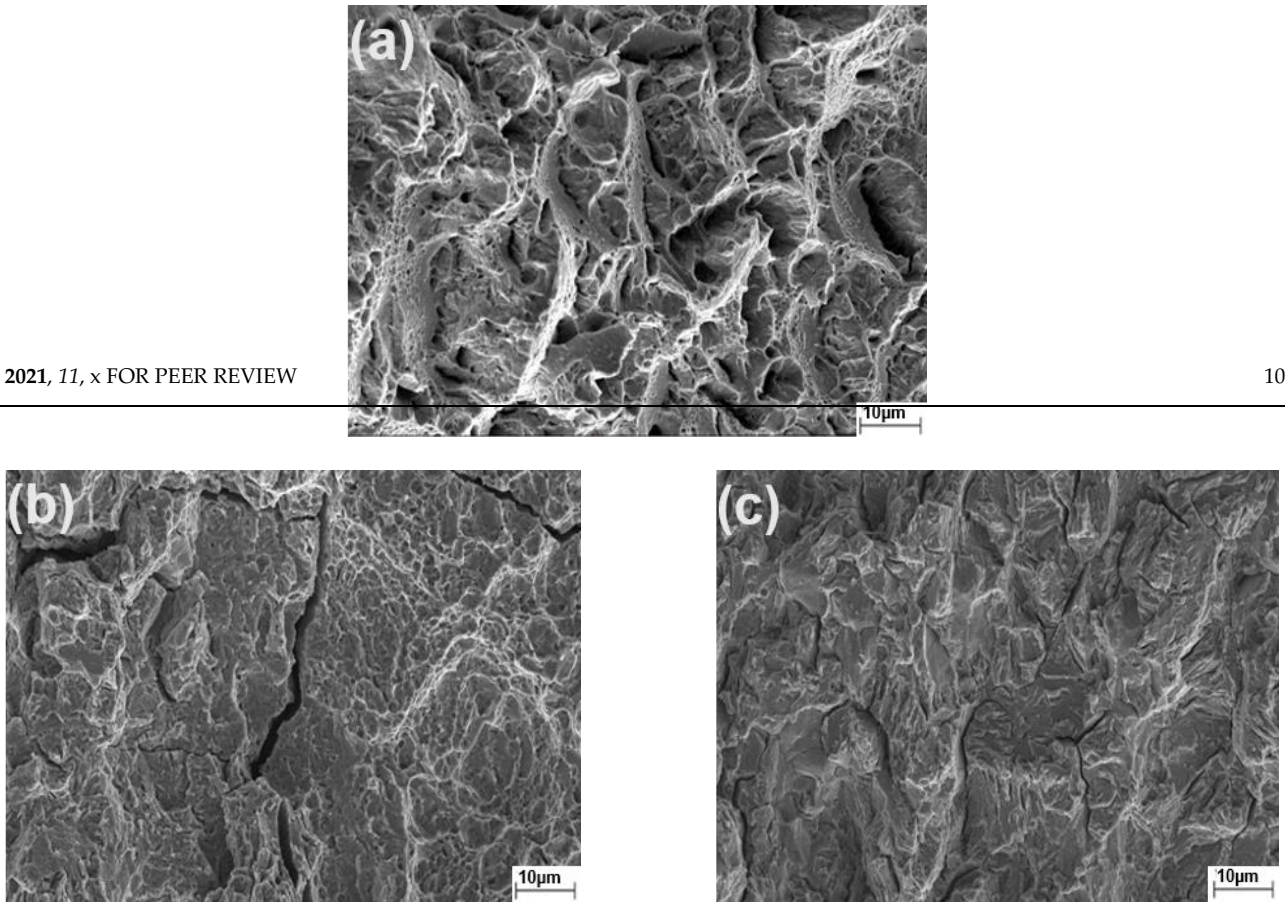

Figure 9. Micrographs of fracture surface for studied steel after CERT with varying hydrogen content: (**a**) In air; (**b**) H charged to 1.1 wt.ppm corresponding to hydrogen critical concentration; (**c**) H charged to 4.8 wt.ppm corresponding to the lower plateau on the embrittlement curve.

4. Discussion

The increase of hydrogen at the surface of the working electrode (specimen in this case) results in higher concentration gradient, which contributes to increased hydrogen uptake by the material as observed in Figure 4b. The reduction of measured hydrogen concentration observed after 1.3 V_{SCE} can be ascribed to the effect of hydrogen gas bubbling at the specimen surface. The bubbles which stick to the specimen surface reduce markedly the effective contact area between metal and the electrolyte, producing hydrogen of high fugacity for its adsorption into the metal surface.

The performance of the steel under CERT in the presence of hydrogen is reported in Figure 5b. Similar phenomenon of the embrittlement curve has been reported for martensitic steels grades with varying strengths, hardness, and microstructures [21,22]. The critical hydrogen concentration (H_{crit} = 1.1 wt.ppm) determined for the studied steel is comparatively higher than that determined for USIBOR 2000 (H_{crit} = 0.6 wt.ppm) and USIBOR 1500 (H_{crit} = 0.8 wt.ppm) [21], but similar to that determined for M1400 (H_{crit} = 1 wt.ppm) [22].

In hydrogen-steel interactions, hydrogen enters the steel, diffuses through the lattice preferably along the grain boundaries, interacts with microstructural features and defects, moves with mobile dislocations, and modifies the steel property under external load, resulting in quasi-cleavage and intergranular fracture modes. Specifically, failure occurs when hydrogen concentration in the steel reaches a certain critical value, which is a prerequisite for most proposed hydrogen embrittlement mechanisms [7,20]. Considering that hydrogen in steels interacts preferably with specific microstructural features and defects, it is essential to distinguish between different critical concentrations reported in literature as: (a) Global total hydrogen concentration in the bulk steel specimen after fracture and (b) hydrogen concentration at a particular location in the steel that is sufficient enough to initiate cracking leading to failure [41]. In fact, the abrupt drop in local strength and ductility upon reaching the critical concentration is mostly responsible for the change in frac-

degradation, is caused by the presence of hydrogen. Additionally, the density of hydrogen-induced secondary cracks were determined by linear intercept method to have increased by a factor of two for the specimen charged to critical concentration compared to the hydrogen free sample. Similar observations were made in martensitic steels by Lovicu et al. [22], where secondary cracks induced by electrochemical charging generally lower the steel strength. Admitting that the secondary cracks do not have the same morphology or extension, their contribution to the susceptibility of the steel at stresses corresponding to critical hydrogen concentration cannot be dismissed.

Further fractographic observations were performed on the post-tensile specimens that fractured upon reaching the hydrogen critical concentration (about 1.1 wt.ppm) on the embrittlement curve, to highlight the main factors influencing the susceptibility to hydrogen of the steel. The majority of the hydrogen-induced cracks leading to failure have been found to nucleate from high stress concentration regions, such as the white-dashed marked feature in Figure 11a. Further investigation shows that those stress concentration regions were characterized by inclusion particles. Figure 11b shows micrographs of one post-tensile specimen charged to 1.1 wt.ppm, where the crack initiates from the alumina particle (emphasized by yellow arrow) leading to failure. The results from energy-dispersive spectroscopy (EDS) on the particles revealed them to be mostly aluminum-based non-metallic inclusions (NMI), as shown in Figure 11c. Even though stress concentration always plays a significant role in fracture of steels, even without hydrogen, the deleterious contribution of hydrogen to the loss of steel strength is markedly enhanced [20,22,37,40].

It is difficult to assert concretely that the fracture of steels upon reaching measured hydrogen critical concentration is due to only local or total average hydrogen activity in the steel. However, the synergic interplay between local hydrogen concentrations and local stress states accompanied with total average hydrogen presence reducing the general plasticity of the specimen, should be responsible for the observed degradation of strength of the steel around the critical concentration zone on the embrittlement curve. Despite, in literature, the term critical hydrogen concentration, in its definition, being more related to the local concentration of hydrogen responsible for crack nucleation, its measurement is difficult, as it may have diffused out of the sample at the actual time of the fracture [20,41].

in literature as: (a) Global total hydrogen concentration in the bulk steel specimen after fracture and (b) hydrogen concentration at a particular location in the steel that is sufficient enough to initiate cracking leading to failure [41]. In fact, the abrupt drop in local strength and ductility upon reaching the critical concentration is mostly responsible for the change in fracture mode from ductile to brittle. Even so, the contribution of the total average hydrogen content to the susceptibility of the steel cannot be totally ruled out.

An evidence of the contribution of global content of hydrogen to failure at the stresses corresponding to critical concentration can be ascertained by observing the fracture surfaces for post-tensile in air of the specimen tested in as-supplied condition, depicted in Figure 10a, and hydrogen charged to 1.1 wt.ppm, as showed in Figure 10b. The fracture surface of the specimen tested in air shows a reduction of fractured surface area from 5 to 3 mm^2 (i.e., of about 40%), which evidences necking prior to fracture. This reduction of area is absent from the fracture surface of the specimen tested under continuous hydrogen charging to attain critical concentrations. It is possible to assert that the absence of reduction in area in the charged specimen, implying the loss of ductility as result of hydrogen critical concentration is due to only local or total average hydrogen activity in the steel. However, the synergic interplay between local hydrogen concentrations and local stress states accompanied with total average hydrogen presence reducing the general plasticity of the specimen, should be responsible for the observed degradation of strength of the steel around the critical concentration zone on the embrittlement curve. Despite, in literature, the term critical hydrogen concentration, in its definition, being more related to the local concentration of hydrogen responsible for crack nucleation, its measurement is difficult, as it may have diffused out of the sample at the actual time of the fracture [20,41].

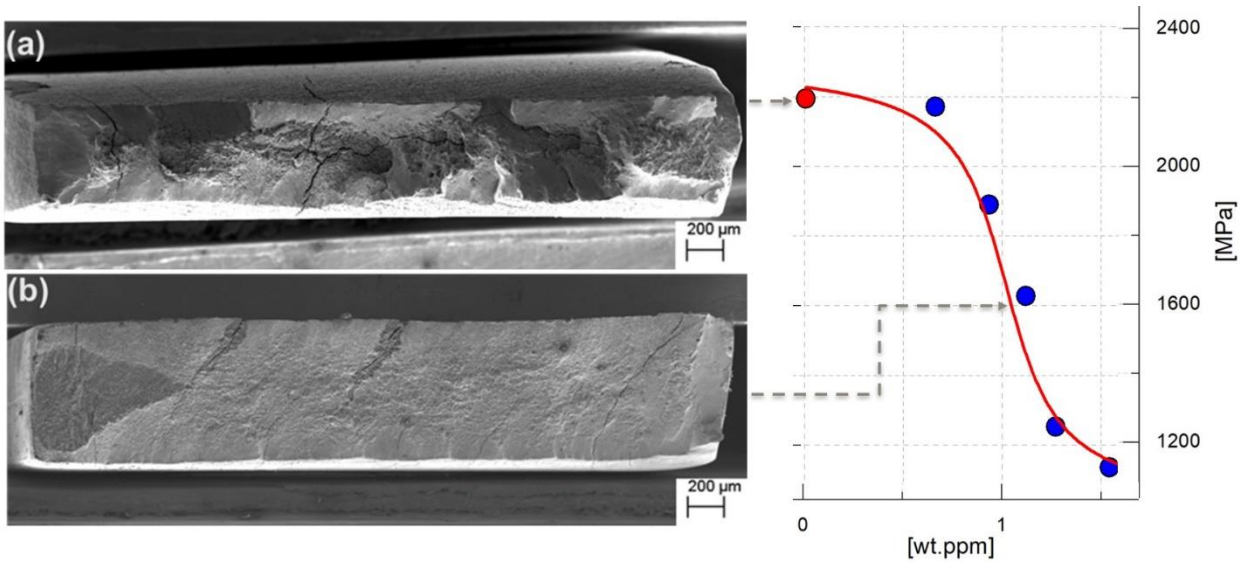

Figure 10. Fracture surface of the tensile specimens: (**a**) Tested in air without hydrogen charging; (**b**) electrochemical hydrogen charged to 1.1 wt.ppm.

Figure 10. Fracture surface of the tensile specimens: (**a**) Tested in air without hydrogen charging; (**b**) electrochemical hydrogen charged to 1.1 wt.ppm.

Further fractographic observations were performed on the post-tensile specimens that fractured upon reaching the hydrogen critical concentration (about 1.1 wt.ppm) on the embrittlement curve, to highlight the main factors influencing the susceptibility to hydrogen of the steel. The majority of the hydrogen-induced cracks leading to failure have been found to nucleate from high stress concentration regions, such as the white-dashed marked feature in Figure 11a. Further investigation shows that those stress concentration regions were characterized by inclusion particles. Figure 11b shows micrographs of one post-tensile specimen charged to 1.1 wt.ppm, where the crack initiates from the alumina particle (emphasized by yellow arrow) leading to failure. The results from energy-dispersive spectroscopy (EDS) on the particles revealed them to be mostly aluminum-based

Metals **2021**, *11*, x FOR PEER REVIEW 12 of 16

non-metallic inclusions (NMI), as shown in Figure 11c. Even though stress concentration always plays a significant role in fracture of steels, even without hydrogen, the deleterious contribution of hydrogen to the loss of steel strength is markedly enhanced [20,22,37,40].

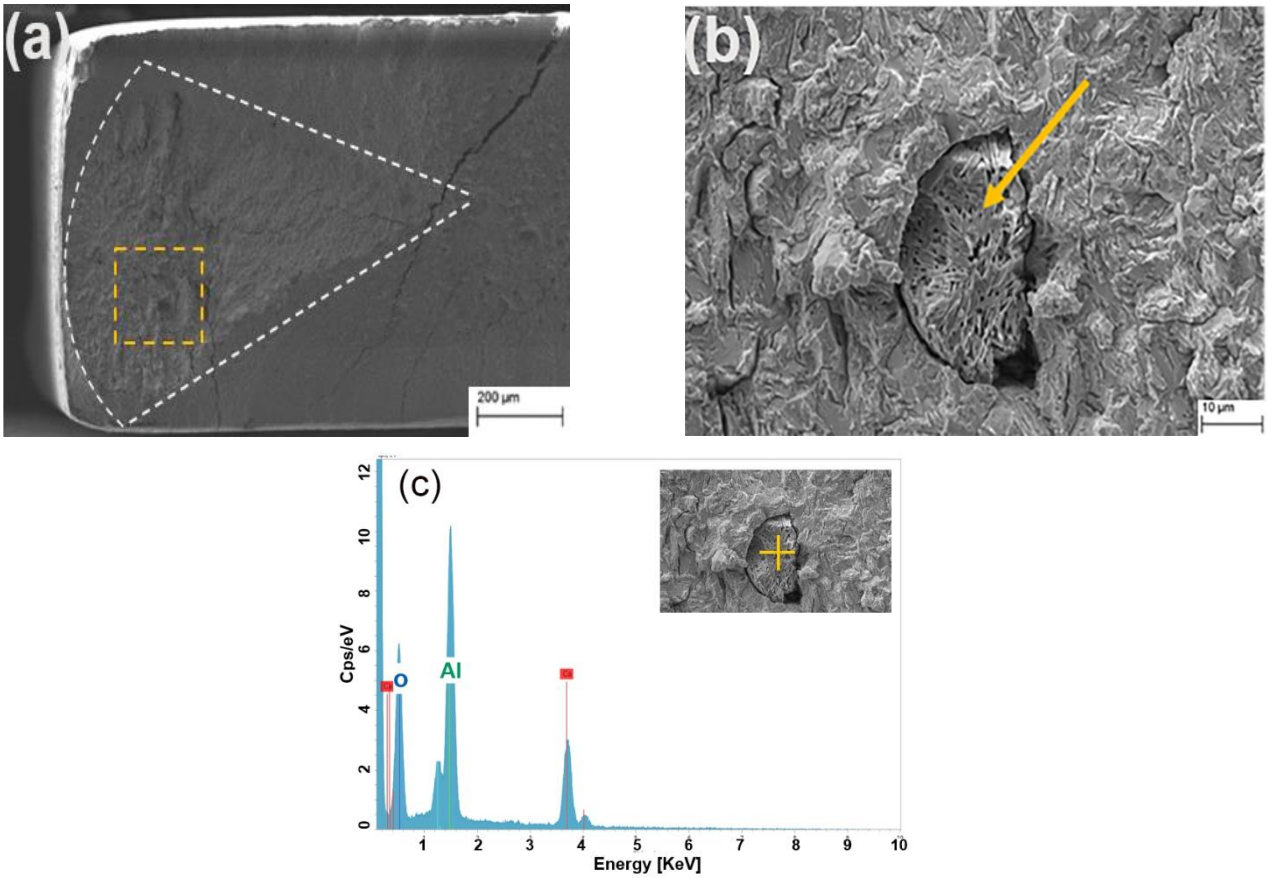

Figure 11. (**a**) Fractography of the specimen charged to 11 wt.ppm; (**b**) higher magnification of the yellow square in (**a**) showing the initiation from an inclusion; (**c**) energy dispersive spectroscopy (EDS) to be (EDS) to be an Al_2O_3 particle.

CLT were performed, at varying loads under continuous electrochemical hydrogen charging, after 2 h of pre-charging with parameters sufficient to provide the critical concentration of hydrogen in the studied steel. It was reported [7,20] that hydrogen in steels exposed to constant load segregates and modifies the stress fields of dislocations, enhancing their movement at lower stress levels. The enhanced movement of dislocation may be responsible for the observed increase in creep rates, with increasing hydrogen content corresponding to the proposed hydrogen enhanced local plasticity (HELP) mechanism [7,19,42].

It is difficult to assert correctly that the fracture of steels upon reaching measured hydrogen critical concentration is due to only local or total average hydrogen activity in the steel. However, the synergic interplay between local hydrogen concentrations and local stress states, accompanied with total average hydrogen presence reducing the general plasticity of the specimen, should be responsible for the observed degradation of strength of the steel around the critical concentration zone on the embrittlement curve. Despite, in literature, the term critical hydrogen concentration, in its definition, being more related to the local concentration of hydrogen responsible for crack nucleation, its measurement is difficult, as it may have diffused out of the sample at the actual time of the fracture [20,41].

CLT were performed, at varying loads under continuous electrochemical hydrogen charging, after 2 h of pre-charging with parameters sufficient to provide the critical concentration of hydrogen in the studied steel. It was reported [7,20] that hydrogen in steels exposed to constant load segregates and modifies the stress fields of dislocations, enhancing their movement at lower stress levels. The enhanced movement of dislocation may be responsible for the observed increase in creep rates, with increasing hydrogen content corresponding to the proposed hydrogen enhanced local plasticity (HELP) mechanism [7,19,42].

It is worth noting that the experimental data points in Figure 8b were obtained at different applied loads. Hence the possibility that the increase in creep rates may not only be primarily due to increasing hydrogen but also increasing loads. Whereas increasing loads are a contributing factor to increased measured hydrogen for specimens charged using the same parameters. Higher applied loads result into more deformation, enhancing the ability to uptake more hydrogen. To eliminate the increasing contribution of applied loads on the creep rates, further CLT were conducted at the same applied load, corresponding to a stress level of 1400 MPa: (i) in air, (ii) in hydrogen charging conditions providing lower hydrogen content than the critical concentration, and (iii) in hydrogen charging expected to provide about the critical concentration of hydrogen. The results are summarized in Table 2.

It is worth noting that the experimental data points in Figure 8b were obtained at different applied loads. Hence the possibility that the increase in creep rates may not only be primarily due to increasing hydrogen but also increasing loads. Whereas increasing loads

Metals **2021**, *11*, x FOR PEER REVIEW

are a contributing factor to increased measured hydrogen for specimens charged using the same parameters. Higher applied loads result into more deformation, enhancing the ability to uptake more hydrogen. To eliminate the increasing contribution of applied loads on the creep rates, further CLT were conducted at the same applied load, corresponding to a stress level of 1400 MPa: (i) In air, (ii) in hydrogen charging conditions providing lower hydrogen content than the critical concentration, and (iii) in hydrogen charging expected to provide about the critical concentration of hydrogen. The results are summarized in Table 2.

Table 2. Effect of increasing critical hydrogen content on creep rates during constant load tests.

Sample ID	H-Charging Parameters [V_{SCE}]	Electrolyte (3% NaCl + 0.1% NH_4SCN)	Measured Hydrogen Content [wt.ppm]	Creep Rates [mm/(mm.min)]
A	n.a.	no	0.5	2.51×10^{-7}
B	−0.8	yes	0.67	7.03×10^{-7}
C	−1.0	yes	1.04	7.85×10^{-5}

Table 2. Effect of increasing critical hydrogen content on creep rates during constant load tests.

Sample ID	H-Charging Parameters [V_{SCE}]	Electrolyte (3% NaCl + 0.1% NH_4SCN)	Measured Hydrogen Content [wt.ppm]	Creep Rates [mm/(mm.min)]	Time to Fracture [h]
A	n.a.	no	0.5	2.51×10^{-7}	No fracture
B	−0.8	yes	0.67	7.03×10^{-7}	0.11
C	−1.0	yes	1.04	7.85×10^{-5}	0.52

Sample A did not fracture after 85 h, while samples B and C were fractured after 11 and 0.52 h under load, respectively. As shown in Figure 12, the increase of hydrogen content up to the critical concentration increases markedly the creep rates by more than two orders of magnitude in the studied steel under the same loads. This is comparable with values reported for different grades of cast iron [40] where creep rates increased for hydrogen charged samples as compared to that tested in distilled water. It is important to note that the effects of critical hydrogen concentration on creep rates may be dependent on experimental conditions, especially strain rates used to attain the constant load regime, but this need more investigation beyond the scope of the present publication; more work is required to ascertain effective methods that can enhance the HE susceptibility of the studied steel. It has been suggested that suitable tempering after hot rolling could be applied to enhance the HE properties as well as to obtain maximum mechanical properties [43]; however, this requires further investigation to ascertain its effectiveness for the studied steel.

Sample A did not fracture after 85 h, while samples B and C were fractured after 11 and 0.52 h under load, respectively. As shown in Figure 12, the increase of hydrogen content up to the critical concentration increases markedly the creep rates by more than two orders of magnitude in the studied steel under the same loads. This is comparable with values reported for different grades of cast iron [40] where creep rates increased for hydrogen charged samples as compared to that tested in distilled water. It is important to note that the effects of critical hydrogen concentration on creep rates may be dependent on experimental conditions, especially strain rates used to attain the constant load regime, but this need more investigation beyond the scope of the present publication; more work is required to ascertain effective methods that can enhance the HE susceptibility of the studied steel. It has been suggested that suitable tempering after hot rolling could be applied to enhance the HE properties as well as to obtain maximum mechanical properties [43]; however, this requires further investigation to ascertain its effectiveness for the studied steel.

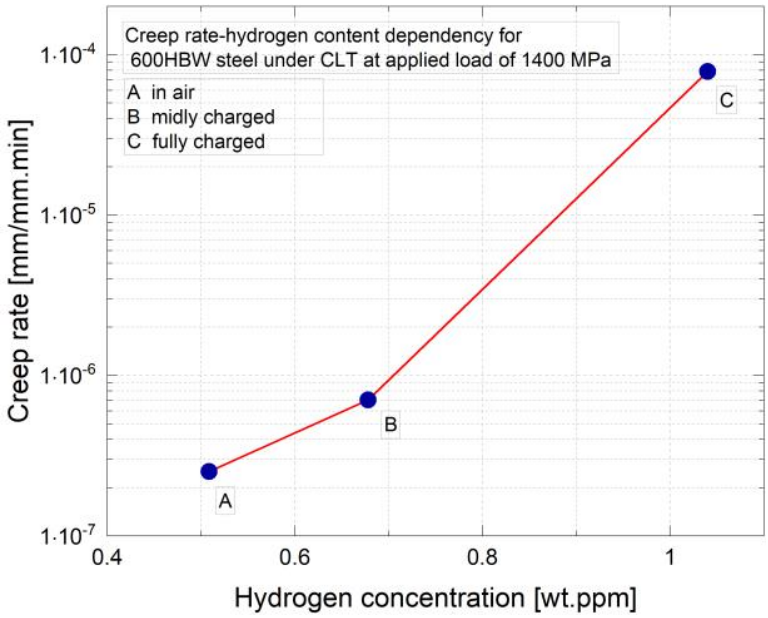

Figure 12. Creep rates in CLT under applied stress of 1400 MPa as a function of measured hydrogen concentration.

Figure 12. Creep rates in CLT under applied stress of 1400 MPa as a function of measured hydrogen concentration.

5. Conclusions

The effects of hydrogen on mechanical performance of a 600 HBW m
were evaluated through CERT and CLT under continuous hydrogen cha
lowing is worth highlighting:

5. Conclusions

The effects of hydrogen on mechanical performance of a 600 HBW martensitic steel were evaluated through CERT and CLT under continuous hydrogen charging. The following is worth highlighting:

- The strength of the martensitic steel reduces from an apparent upper plateau for small hydrogen contents to a clear lower plateau at about 1100 MPa for hydrogen concentrations higher than 2 wt.ppm. This about 50% tensile strength degradation, at the lower plateau, stays essentially constant for hydrogen concentrations up to 4.8 wt.ppm. Thus, the observed lower plateau can be considered as the maximum hydrogen effect on the UTS of the studied steel.
- The critical hydrogen concentration found was 1.1 wt.ppm, corresponding to the midpoint between the upper and lower strength plateaus. At this point, the degradation of tensile strength is about 25% of the original UTS.
- In the CLT of the uncharged condition of the steel, no fracture occurred at applied load up to 72% of UTS. In continuous hydrogen charged samples, at conditions providing the critical hydrogen concentrations of 1.1 wt.ppm, the steel fracture occurred at 85 h under applied load of 50% of UTS.
- The presence of hydrogen at 0.65 and 1.04 wt.ppm (i.e., below the critical hydrogen concentration of 1.1 wt.ppm) increased, markedly, the creep rates during CLT by more than two orders of magnitude, under same loads, compared to uncharged specimens.
- Although more work is required towards a deep assessment of the influence of the microstructure in the mechanism driving the HE, the largely dominant martensitic microstructure, with only a small fraction of bainitic islands and corresponding bainite/martensite interfaces, may be the reason for the observed lower plateau and apparent saturation of the effect of hydrogen in this 600 HBW steel. Ongoing research in similar hard steels, with higher fraction of bainite, is expected to provide further support to this conclusion.

Author Contributions: Conceptualization, data curation, visualization, formal analysis, and writing—original draft preparation, E.F.; methodology, E.F. and Y.Y.; investigation, E.F. and E.M.; resources, S.M. and E.V.; and editing, E.F., Y.Y., E.M. and P.V.; project administration, supervision, review and editing, P.V.; funding acquisition, Y.Y. and P.V. All authors have read and agreed to the published version of the manuscript.

Funding: This researcher was supported by the Public Research Networked with Companies (Co-Innovation) program of Business Finland via the projects 7743/31/2018 (ISA Aalto-HydroSafeSteels) and 7537/31/2018 (ISA-Intelligent Steel Applications).

Institutional Review Board Statement: Not applicable.

Informed Consent Statement: Not applicable.

Data Availability Statement: Not applicable.

Acknowledgments: The authors wish to acknowledge Kim Widell, Jyrki Romu and Laura Tiainen for their technical support.

Conflicts of Interest: The authors declare no conflict of interest.

References

1. Hardox Wear Plate. The Extra Hard and Tough Steel for Extreme Wear. Available online: https://www.ssab.com/products/brands/hardox/products/hardox-600 (accessed on 19 May 2021).
2. Armox Protection Plate, Ramor® 600. The Ballistic Protection Steel with Extra-High Hardness. Available online: https://www.ssab.com/products/brands/armox/ramor-600 (accessed on 24 May 2021).
3. Djukic, M.B.; Bakic, G.M.; Zeravcic, V.S.; Sedmak, A.; Rajicic, B. Hydrogen embrittlement of industrial components: Prediction, prevention, and models. *Corrosion* **2016**, *72*, 943–961. [CrossRef]
4. Djukic, M.B.; Zeravcic, V.S.; Bakic, G.M.; Sedmak, A.; Rajicic, B. Hydrogen damage of steels: A case study and hydrogen embrittlement model. *Eng. Fail. Anal.* **2015**, *58*, 485–498. [CrossRef]

5. Rogers, H.C. Hydrogen Embrittlement of Metals: Atomic hydrogen from a variety of sources reduces the ductility of many metals. *Science* **1968**, *159*, 1057–1064. [CrossRef]
6. Akiyama, E.; Wang, M.; Li, S.; Zhang, Z.; Kimura, Y.; Uno, N.; Tsuzaki, K. Studies of Evaluation of Hydrogen Embrittlement Property of High-Strength Steels with Consideration of the Effect of Atmospheric Corrosion. *Metall. Mater. Trans. A* **2013**, *44*, 1290–1300. [CrossRef]
7. Robertson, I.M.; Sofronis, P.; Nagao, A.; Martin, M.L.; Wang, S.; Gross, D.W.; Nygren, K.E. Hydrogen embrittlement understood. *Metall. Mater. Trans. A* **2015**, *46*, 2323–2341. [CrossRef]
8. Dayal, R.K.; Parvathavarthini, N. Hydrogen embrittlement in power plant steels. *Sadhana* **2003**, *28*, 431–451. [CrossRef]
9. Oriani, R.A.; Josephic, P.H. Testing of the decohesion theory of hydrogen-induced crack propagation. *Scr. Metall.* **1972**, *6*, 681–688. [CrossRef]
10. Stahle, R.W.; Hochmann, J.; McCright, R.D.; Slater, J.E.; Shatynski, S.R. Stress corrosion cracking and hydrogen embrittlement of iron base alloys. *J. Electrochem. Soc.* **1979**, *126*, 215C. [CrossRef]
11. Hardie, D.; Charles, E.A.; Lopez, A.H. Hydrogen embrittlement of high strength pipeline steels. *Corros. Sci.* **2006**, *48*, 4378–4385. [CrossRef]
12. Sandoz, G. A unified theory for some effects of hydrogen source, alloying elements, and potential on crack growth in martensitic AISI 4340 steel. *Metall. Trans.* **1972**, *3*, 1169–1176. [CrossRef]
13. Hudgins, C.M.; McGlasson, R.L.; Mehdlzadeh, P.; Rosborough, W.M. Hydrogen sulfide cracking of carbon and alloy steels. *Corrosion* **1966**, *22*, 238–251. [CrossRef]
14. Brahimi, S.V.; Yue, S.; Sriraman, K.R. Alloy and composition dependence of hydrogen embrittlement susceptibility in high-strength steel fasteners. *Philos. Trans. Ser. A Math. Phys. Eng. Sci.* **2017**, *375*, 20160407. [CrossRef] [PubMed]
15. Fangnon, E.; Malitckii, E.; Yagodzinskyy, Y.; Vilaça, P. Improved accuracy of thermal desorption spectroscopy by specimen cooling during measurement of hydrogen concentration in a high-strength steel. *Materials* **2020**, *13*, 1252. [CrossRef] [PubMed]
16. Zapffe, C.A.; Sims, C.E. Hydrogen embrittlement, internal stress and defects in steel. *Trans. AIME* **1941**, *145*, 225–271.
17. Gangloff, R.P.; Somerday, B.P. *Gaseous Hydrogen Embrittlement of Materials in Energy Technologies: The Problem, Its Characterisation and Effects on Particular Alloy Classes*; Elsevier: Amsterdam, The Netherlands, 2012.
18. Liu, Q.; Atrens, A.D.; Shi, Z.; Verbeken, K.; Atrens, A. Determination of the hydrogen fugacity during electrolytic charging of steel. *Corros. Sci.* **2014**, *87*, 239–258. [CrossRef]
19. Depover, T.; Verbeken, K. The detrimental effect of hydrogen at dislocations on the hydrogen embrittlement susceptibility of Fe-CX alloys: An experimental proof of the HELP mechanism. *Int. J. Hydrog. Energy* **2018**, *43*, 3050–3061. [CrossRef]
20. Djukic, M.B.; Bakic, G.M.; Sijacki Zeravcic, V.; Sedmak, A.; Rajicic, B. The synergistic action and interplay of hydrogen embrittlement mechanisms in steels and iron: Localized plasticity and decohesion. *Eng. Fract. Mech.* **2019**, *216*, 106528. [CrossRef]
21. Valentini, R.; Tedesco, M.M.; Corsinovi, S.; Bacchi, L.; Villa, M. Investigation of mechanical tests for hydrogen embrittlement in automotive PHS steels. *Metals* **2019**, *9*, 934. [CrossRef]
22. Lovicu, G.; Bottazzi, M.; D'aiuto, F.; De Sanctis, M.; Dimatteo, A.; Santus, C.; Valentini, R. Hydrogen embrittlement of automotive advanced high-strength steels. *Metall. Mater. Trans. A* **2012**, *43*, 4075–4087. [CrossRef]
23. Wang, M.; Akiyama, E.; Tsuzaki, K. Determination of the critical hydrogen concentration for delayed fracture of high strength steel by constant load test and numerical calculation. *Corros. Sci.* **2006**, *48*, 2189–2202. [CrossRef]
24. Takagi, S.; Inoue, T.; Hara, T.; Hayakawa, M.; Tsuzaki, K.; Takahashi, T. Parameters for the evaluation of hydrogen embrittlement of high strength steel. *Tetsu-Hagané* **2000**, *86*, 689–696. [CrossRef]
25. Wang, M.; Akiyama, E.; Tsuzaki, K. Fracture criterion for hydrogen embrittlement of high strength steel. *Mater. Sci. Technol.* **2006**, *22*, 167–172. [CrossRef]
26. Akiyama, E.; Li, S.; Zhang, Z.; Wang, M.; Matsukado, K.; Tsuzaki, K. National Institute for Materials Science, Tsukuba, Ibaraki, Japan, Boping Zhang, University of Science and Technology Beijing, Beijing, China Hydrogen Embrittlement of High Strength Steels and Environmental Hydrogen Entry. In *Effects of Hydrogen on Materials, Proceedings of the 2008 International Hydrogen Conference, (ASM International) 2009, Materials Park, OH, USA, 7–10 September 2008*; pp. 54–61. Available online: http://www.asminternational.org/portal/site/www/AsmStore/ProductDetails/?vgnextoid=132dbeec8c236210VgnVCM100000621e010aRCRD (accessed on 22 January 2021).
27. Lee, D.; Sun, B.; Lee, S.; Ponge, D.; Jägle, E.A.; Raabe, D. Comparative study of hydrogen embrittlement resistance between additively and conventionally manufactured 304L austenitic stainless steels. *Mater. Sci. Eng. A* **2021**, *803*, 140499. [CrossRef]
28. Baek, S.; Song, E.J.; Kim, J.H.; Jung, M.; Baek, U.B.; Nahm, S.H. Hydrogen embrittlement of 3-D printing manufactured austenitic stainless steel part for hydrogen service. *Scr. Mater.* **2017**, *130*, 87–90. [CrossRef]
29. Wang, M.; Akiyama, E.; Tsuzaki, K. Effect of hydrogen on the fracture behavior of high strength steel during slow strain rate test. *Corros. Sci.* **2007**, *49*, 4081–4097. [CrossRef]
30. Wang, M.; Akiyama, E.; Tsuzaki, K. Effect of hydrogen and stress concentration on the notch tensile strength of AISI 4135 steel. *Mater. Sci. Eng. A* **2005**, *398*, 37–46. [CrossRef]
31. Takagi, S.; Terasaki, S.; Tsuzaki, K.; Inoue, T.; Minami, F. A new evaluation method of hydrogen embrittlement fracture for high strength steel by local approach. *ISIJ Int.* **2005**, *45*, 263–271. [CrossRef]
32. Wang, M.; Akiyama, E.; Tsuzaki, K. Hydrogen degradation of a boron-bearing steel with 1050 and 1300 MPa strength levels. *Scr. Mater.* **2005**, *52*, 403–408. [CrossRef]

33. Wang, M.; Akiyama, E.; Tsuzaki, K. Crosshead speed dependence of the notch tensile strength of a high strength steel in the presence of hydrogen. *Scr. Mater.* **2005**, *53*, 713–718. [CrossRef]
34. Takagi, S.; Inoue, T.; Tsuzaki, K.; Minami, F. Determination method of Weibull shape parameter for evaluation of the hydrogen embrittlement susceptibility of high strength steel. *Nippon Kinzoku Gakkaishi* **2001**, *65*, 1082–1090.
35. Takagi, S.; Toji, Y. Application of NH4SCN aqueous solution to hydrogen embrittlement resistance evaluation of ultra-high strength steels. *ISIJ Int.* **2012**, *52*, 329–331. [CrossRef]
36. Beghini, M.; Benamati, G.; Bertini, L.; Ricapito, I.; Valentini, R. Effect of hydrogen on the ductility reduction of F82H martensitic steel after different heat treatments. *J. Nucl. Mater.* **2001**, *288*, 1–6. [CrossRef]
37. Todoshchenko, O.; Yagodzinskyy, Y.; Yagodzinska, V.; Saukkonen, T.; Hänninen, H. Hydrogen effects on fracture of high-strength steels with different micro-alloying. *Corros. Rev.* **2015**, *33*, 515–527. [CrossRef]
38. Koyama, M.; Rohwerder, M.; Tasan, C.C.; Bashir, A.; Akiyama, E.; Takai, K.; Raabe, D.; Tsuzaki, K. Recent progress in microstructural hydrogen mapping in steels: Quantification, kinetic analysis, and multi-scale characterisation. *Mater. Sci. Technol.* **2017**, *33*, 1481–1496. [CrossRef]
39. Lu, R.; Minami, I.; Nanao, H.; Mori, S. Investigation of decomposition of hydrocarbon oil on the nascent surface of steel. *Tribol. Lett.* **2007**, *27*, 25–30. [CrossRef]
40. Forsström, A.; Yagodzinskyy, Y.; Hänninen, H. Hydrogen effects on mechanical performance of nodular cast iron. *Corros. Rev.* **2019**, *37*, 441–454. [CrossRef]
41. Dadfarnia, M.; Nagao, A.; Wang, S.; Martin, M.L.; Somerday, B.P.; Sofronis, P. Recent advances on hydrogen embrittlement of structural materials. *Int. J. Fract.* **2015**, *196*, 223–243. [CrossRef]
42. Lynch, S.P. Hydrogen embrittlement (HE) phenomena and mechanisms. In *Stress Corrosion Cracking*; Elsevier: Amsterdam, The Netherlands, 2011; pp. 90–130.
43. Zhang, Y.; Xu, Z.; Zhao, X.; Gao, G.; Hui, W.; Weng, Y. Hydrogen embrittlement behavior of high strength bainitic rail steel: Effect of tempering treatment. *Eng. Fail. Anal.* **2018**, *93*, 100–110. [CrossRef]